Inorganic Chemistry

Article

pubs.acs.org/IC

Design of a Dinuclear Nickel(II) Bioinspired Hydrolase to Bind Covalently to Silica Surfaces: Synthesis, Magnetism, and Reactivity Studies

Clovis Piovezan,[†] Jaqueline M. R. Silva,[†] Ademir Neves,*[,†] Adailton J. Bortoluzzi,[†] Wolfgang Haase,[‡] Zbigniew Tomkowicz,[§] Eduardo E. Castellano,[∥] Tessa C. S. Hough,[⊥] and Liane M. Rossi*[,⊥]

[†]Departamento de Química, Laboratório de Química Bioinorgânica e Cristalografia (LABINC), Universidade Federal de Santa Catarina, SC, 88040-900 Florianópolis, Brazil

[‡]Institut für Physikalische Chemie, Technische Universität Darmstadt, Petersenstrasse 20, D-64287-Darmstadt, Germany

[§]Institute of Physics, Reymonta 4, Jagiellonian University, PL-30-059 Krakow, Poland

[∥]Instituto de Física, Universidade Federal de São Carlos, São Carlos, SP 13560-970, Brazil

[⊥]Instituto de Química, Universidade de São Paulo, São Paulo 05508-000, Brazil

Supporting Information

ABSTRACT: Presented herein is the design of a dinuclear Ni^{II} synthetic hydrolase $[Ni_2(HBPPAMFF)(\mu\text{-}OAc)_2(H_2O)]\text{-}BPh_4$ (**1**) ($H_2BPPAMFF$ = 2-[(*N*-benzyl-*N*-2-pyridylmethyl-amine)]-4-methyl-6-[*N*-(2-pyridylmethyl)aminomethyl)])-4-methyl-6-formylphenol) to be covalently attached to silica surfaces, while maintaining its catalytic activity. An aldehyde-containing ligand ($H_2BPPAMFF$) provides a reactive functional group that can serve as a cross-linking group to bind the complex to an organoalkoxysilane and later to the silica surfaces or directly to amino-modified surfaces. The dinuclear Ni^{II} complex covalently attached to the silica surfaces was fully characterized by different techniques. The catalytic turnover number (k_{cat}) of the immobilized $Ni^{II}Ni^{II}$ catalyst in the hydrolysis of 2,4-bis(dinitrophenyl)phosphate is comparable to the homogeneous reaction; however, the catalyst interaction with the support enhanced the substrate to complex association constant, and consequently, the catalytic efficiency ($E = k_{cat}/K_M$) and the supported catalyst can be reused for subsequent diester hydrolysis reactions.

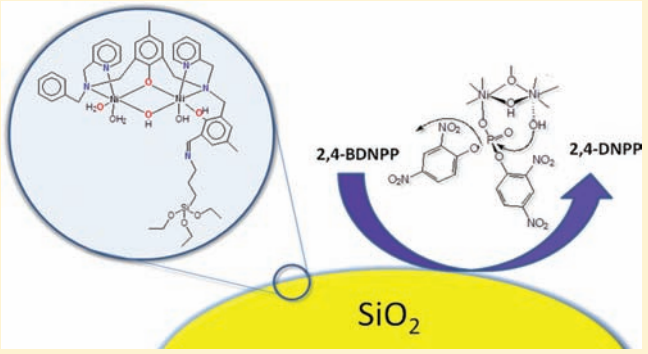

INTRODUCTION

The development of unsymmetrical polydentate ligands and their use for the preparation of mono- and dinuclear metal complexes with catalytic activity as metallohydrolases and/or metalloproteases are examples of synthetic bioinspired systems.[1,2] Nucleases are natural catalysts much more efficient and specific than those synthesized in the laboratory and their biological role includes the degradation or digestion of polymers, modification of nucleic acids, DNA repair, and viral defense (restrictive enzymes).[3] For many nucleases, the metal ions are essential cofactors and are directly involved in the hydrolysis of phosphodiesters. They increase the catalytic rate of the hydrolytic cleavage of the phosphodiester bond by a factor of 10^{12} with respect to the noncatalyzed reaction.[4] The effectiveness of metal ions in promoting the hydrolysis of phosphate bonds and DNA cleavage in biological systems is a function of many factors, including the nature of the metal ion, the phosphatediester species, and the compositions and structures of complexes formed between them. The availability of a nucleophile, such as a properly positioned coordinated metal-hydroxide, is critical to an effective hydrolysis process.[5−12]

The search for low molecular weight molecules able to catalytically cleave DNA has attracted much interest among scientists, although a great number of nucleases are well-known. This interest embraces the elucidation of the cleavage mechanism, the role of metals in biological systems, and the design of more effective synthetic hydrolases, as well as the use of these new compounds as catalysts, conformational probes, and synthetic restriction enzymes.[13]

The study of the catalytic activity of synthetic metallocomplexes in solution, inspired by the catalytic properties of biological systems, has been reported by several groups who found that these substances provide very efficient systems for catalytic oxidation reactions,[14−16] controlled drugs delivery,[17−19] biodiesel transesterification reaction,[20,21] and bleaching process.[22−24]

Received: January 4, 2012
Published: May 15, 2012

   dx.doi.org/10.1021/ic300018t | *Inorg. Chem.* 2012, 51, 6104−6115

A constant theme in these challenging areas is the formation of structured assemblies containing complexes located in well-defined chemical environments. The creation of a supported metal center that is accessible to large organic substrates is an essential property for the biomimetic catalytic application of supported metallocomplexes. The immobilization of metallocomplexes associated with the production of an easily recyclable solid such as an inorganic support; e.g., silica would greatly enhance the usefulness of such complexes for diverse new uses. The combination of efficient catalysts with immobilization on solid supports can result in efficient and selective catalysts because the matrix support can impose shape-selectivity, promoting a special environment for the approach of the substrate to the active species. In addition, immobilization may prevent molecular aggregation or bimolecular self-destruction reactions, which lead to deactivation of the catalytic active species.[25,26]

The immobilization of such biomimetic complexes on the surface of solid supports by covalent bonds rather than by electrostatic attraction requires a step of ligand design. Additionally to the functional groups placed in the ligand to mimic the groups present in the active site (first coordination sphere of the metal) of a given metalloenzyme, the ligand itself should provide a reactive functional group that can serve as a cross-linking group to bind the complex to the solid surface. It is worth drawing the attention to the fact that the changes in the ligand should maintain the corresponding complex properties as expected to mimic the metalloenzyme, such as bond distances and angles. Still, the introduction of reactive functional groups in the ligand must be such that this group will not make part of the coordination sphere of the metal; therefore, the approach of this group to the metal center must be sterically hindered.

In Scheme 1, there is an example of a bioinspired ligand and its dinuclear nickel(II) complex,[27] a biomimetic structural model for nucleases, which displays catalytic activity in hydrolysis of phosphate esters. The complex hydrolyses the substrate bis(2,4-dinitrophenyl)phosphate (2,4-BDNPP) at a rate 138.400 faster than the noncatalyzed reaction at 25 °C and pH 9. Taking into account the structure and activity of this bioinspired nuclease, another ligand has been designed to maintain as much as possible the chemical environment for the metal ions coordination besides the addition of a reactive functional group that can serve as a cross-linking group to bind the corresponding dinuclear Ni^{II} complex to the surface of silica.

Scheme 1. Example of a Bioinspired Synthetic Nuclease[27]

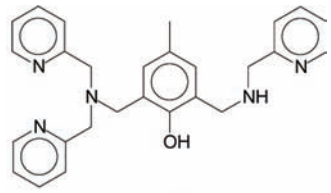

HL1

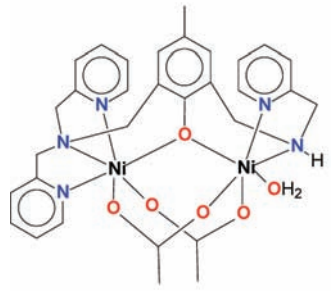

$[Ni_2(L1)(AcO)_2(H_2O)]^+$ - 1

Silica is a very versatile material that can be prepared with good control of particles size and morphology. Sub-100 nm silica nanospheres can be prepared by means of microemulsions,[28,29] or by a modified Stöber sol−gel synthesis,[30] with narrow size distribution. Silica spheres in the nano- and microsize range have been extensively used for the immobilization or entrapment of many kinds of organic molecules, such as dyes,[28,29,31−33] biomolecules,[34−36] DNA,[37] and bioinspired model complexes for nucleases.[38] Silica has been also used for coating different nanomaterials, such as magnetic nanoparticles,[39−42] metal nanoparticles,[43−45] and quantum dots,[46] in order to bring different properties such as chemical stability and easy surface functionalization for targeting purposes. Silica surfaces contain reactive silanol groups that are easy to functionalize by reacting the silica matrix with commercially available organoalkoxysilane reagents[33,47] or organic molecules previously modified with organoalkoxysilane reagents.[48−50] This strategy assures chemical attachment of target molecules to the inorganic matrix by stable covalent bonds.

In this Article, we will describe the design of a dinuclear Ni^{II} synthetic nuclease $[Ni_2(HBPPAMFF)(\mu\text{-}OAc)_2(H_2O)]BPh_4$ (**1**) to be covalently attached to silica surfaces while maintaining its catalytic activity. Interestingly, complex **1** immobilized on functionalized silica has been successfully applied in the construction of a novel sensor for the determination of fisetin by square-wave voltammetry.[51] Herein, experimental details for the syntheses of the ligand H_2BPPAMFF and its dinuclear complex **1** are also described.

EXPERIMENTAL SECTION

Physical Measurements. Electronic spectra were recorded on a Perkin-Elmer UV−Vis/NIR Diode Array spectrophotometer in the 280−800 nm range. IR spectra were recorded on a Bomem MB100 FT-IR spectrometer in the 400−4000 cm^{-1} range. Cyclic voltammetry was performed using an Epsilon EC 2000 Potentiostat (working electrode, gold; reference electrode, Ag/Ag^+; support electrode, platinum; support electrolyte, tetrabutylammonium hexafluorophosphate; internal standard, ferrocene). Elemental analyses were determined on the CHN Perkin-Elmer 2400 analyzer. ^{1}HNMR spectra were recorded on a Varian-FT spectrometer (400 MHz) in $CDCl_3$ using tetramethylsilane as the internal standard. Kinetic measurements were recorded on a Varian Cary 50Bio UV−Vis Diode Array spectrophotometer coupled to a thermostatic bath. Transmission electron microscopy (TEM) images were performed using a Philips CM 200 microscope. Samples for TEM observations were prepared by placing a drop containing the nanoparticles in a carbon-coated copper grid. ESI-MS of the complexes dissolved in ultrapure acetonitrile/water (1:1, v/v) solution (500 μL) were analyzed using an amaZon X Ion Trap MS instrument (Bruker Daltonics) with an ion spray source using electrospray ionization in positive ion mode. The ion source conditions were an ion spray voltage of 4500 V. Nitrogen was used as nebulizing gas (20 psi) and curtain gas (10 psi). The samples were directly infused into the mass spectrometer at a flow rate of 300 μL/h. The scan range was m/z 200−3000. Magnetic DC measurements were performed with a Quantum Design SQUID magnetometer, model MPMS 5XL, in magnetic field of the induction of 0.1 and 2.0 T. No field effect was observed. The measured samples were pure complex **1**, SiO_2-**1**, and pure SiO_2. Additionally, the capsule container was measured.

dx.doi.org/10.1021/ic300018t | Inorg. Chem. 2012, 51, 6104−6115

X-ray Crystallography of Complex 1b. A small fragment with dimensions of 0.05 × 0.02 × 0.02 mm^3 was selected from a crystalline sample of complex **1b** for crystallographic analysis. X-ray diffraction data were measured on a Kappa-CCD diffractometer with graphite-monochromated Mo Kα (λ = 0.71073 Å) radiation, at room temperature. Diffraction data were collected (φ and ω scans with *K*-offsets) with COLLECT.[52] Integration and scaling of the reflections were performed with HKL DENZO-SCALEPACK software package.[53] The unit cell parameters were obtained by least-squares refinement based on the angular settings for all collected reflections using HKL SCALEPACK.[53] Because of the very small size of the crystal, absorption correction was not applied to the intensities. The structure was solved by direct methods[54] and refined by full-matrix least-squares on F^2.[55] All non-hydrogen atoms were refined with anisotropic displacement parameters, except for carbon atoms of one isopropanol solvate. Perchlorate anion is partially disordered in which two oxygen atoms occupy two alternative positions. Water solvate are also disordered. Hydrogen atoms bonded to C atoms were placed at their idealized positions using standard geometric criteria. Just one H atom of the coordinated water molecule was found from the Fourier difference map. H atoms of the isopropanol and water solvate could not be located. Selected crystallographic information is presented in Table 1, and full tables of crystallographic data (except structure factors) were deposited at Cambridge Structural Database (CCDC 843653), and these data are available free of charge at www.ccdc.cam.ac.uk.

Table 1. Crystal Data and Structure Refinement for Complex 1b

empirical formula	$C_{59}H_{70}ClN_5Ni_2O_{15.50}$
formula weight	1250.07
temperature	293(2) K
wavelength	0.71073 Å
crystal system	monoclinic
space group	$P2_1/c$
unit cell dimensions	a = 14.7830(3) Å
	b = 18.4790(6) Å
	c = 22.9010(8) Å
	β = 97.235(2)°
volume	6206.2(3) Å^3
Z	4
density (calculated)	1.338 Mg/m^3
absorption coefficient	0.718 mm^{-1}
F(000)	2624
crystal size	0.05 × 0.02 × 0.02 mm^3
theta range for data collection	2.61 to 25.00°
index ranges	$-17 \le h \le 17$; $-21 \le k \le 18$; $-24 \le l \le 27$
reflections collected	30871
independent reflections	10685 (R_{int} = 0.0725)
absorption correction	none
refinement method	full-matrix least-squares on F^2
data/restraints/parameters	10685/52/764
goodness-of-fit on F^2	1.080
final R indices [$I > 2\sigma(I)$]	R_1 = 0.0915; wR_2 = 0.2436
R indices (all data)	R_1 = 0.1150; wR_2 = 0.2653
largest diff. peak and hole	1.012 and −0.727 e·Å^{-3}

Potentiometric Titrations. The potentiometric studies were carried out with a Corning-350 research pH meter fitted with blueglass and Ag/AgCl reference electrodes, in acetonitrile/water (50:50, v/v) solutions. The pK_w of the acetonitrile/water (50:50% v/v) containing 0.2 mol·L^{-1} of KCl used was 15.40.[56] Equilibrium measurements were performed in a thermostatted cell, purged with argon, containing 50.00 mL of the acetonitrile/water (50:50) solution and 0.05 mmol of complex. The temperature was 25.00 ± 0.05 °C, and the experimental solutions were adjusted to 0.100 mol·L^{-1} of ionic strength by the addition of KCl. Computations of the triplicate results were carried out with the BEST7 program, and species diagrams were obtained with SPE and SPEPLO programs.[57]

Materials. All chemicals were purchased from Aldrich, Sigma, or Merck and were of analytical grade. 2-Chloromethyl-4-methyl-6-formylphenol,[58] 2,4-BDNPP,[59] and 2,4-DNPP[59,60] were synthesized by previously described methods.

Syntheses. *Synthesis of the Ligand 2-[(N-Benzyl-N-2-pyridylmethylamine)]-4-methyl-6-[N-(2-pyridylmethyl)aminomethyl)])-4-methyl-6-formylphenol (H_2BPPAMFF). N-Benzyl-N-2-pyridylmethylamine (BPA).* This amine was synthesized using a procedure similar to that previously described.[61] 2-(Aminomethyl)pyridine (4.9 mL, 47 mmol) was dissolved in 20 mL of methanol and cooled to 0 °C. A methanolic solution of benzaldehyde (5.30 g, 50 mmol, in 30 mL) was added dropwise with stirring. After 24 h, was added carefully sodium tetrahydroborate (1.13 g, 30 mmol) with stirring. The reaction mixture was further stirred for 4 h at room temperature. The mixture was concentrated under reduced pressure, and after the addition of HCl 2 mol·L^{-1} (30 mL), the reaction mixture was washed with 5 × 10 mL of $CHCl_3$ to remove the excess of benzaldehyde. The water layer was made alkaline with saturated aqueous Na_2CO_3 (pH 10), extracted with 5 × 10 mL portions of $CHCl_3$, dried over Na_2SO_4, and concentrated under a reduced pressure. A pale yellow oil was obtained. Yield, 75%. ^{1}H NMR δH (400 MHz; $CDCl_3$): 8.5 [1H, Py]; 7.6−7.1 [8H, Ar]; 3.9−3.8 [4H, CH_2] in ppm.

2-(N-Benzyl-N-2-pyridylmethylamine)-4-methyl-6-formylphenol (BPAMFF). To a solution of BPA (1.5 g, 7.5 mmol in 20 mL of CH_2Cl_2) was slowly added a solution of 2-chloromethyl-4-methyl-6-formylphenol (1.38 g, 7.5 mmol in 30 mL of CH_2Cl_2) under stirring, and the reaction mixture was stirred for 24 h. The desired compound was washed with 5 × 30 mL of saturated aqueous Na_2CO_3 (pH 10), and the organic layer was dried over Na_2SO_4 and concentrated under a reduced pressure. A yellow oil was obtained. Yield: 92%. ^{1}H NMR δH (400 MHz; $CDCl_3$): 10.3 [1H, aldehyde]; 8.5 [1H, Py]; 7.6−7.1 [10H, Ar]; 3.8−3.7 [6H, CH_2]; 2.2 [3H, CH_3] in ppm.

2-[(N-Benzyl-N-2-pyridylmethylamine)]-4-methyl-6-[N-(2-pyridylmethyl)aminomethyl)]phenol (BPAPyFF). A solution of 2-(aminomethyl)pyridine (0.7 mL, 6.7 mmol in 30 mL of CH_3OH) was added dropwise to a solution of the BPAMFF (2.4 g, 6.9 mmol, in 20 mL of CH_3OH) and stirred for 4 h. After 4 h, was added carefully sodium tetrahydroborate (0.25 g, 6.7 mmol) with stirring. The reaction mixture was stirred for another 4 h at room temperature. The mixture was concentrated under a reduced pressure and after added 30 mL of HCl 2 mol·L^{-1}. The aqueous phase was washed with 5 × 10 mL of $CHCl_3$. The water layer was made alkaline by saturated aqueous Na_2CO_3 (pH 10), extracted with five 10 mL portions of $CHCl_3$, dried over Na_2SO_4, and concentrated under a reduced pressure. A yellow oil was obtained. Yield: 72%. ^{1}H NMR δH (400 MHz; $CDCl_3$): 8.5 [2H, Py]; 7.6−6.8 [13H, Ar]; 3.9−3.6 [10H, CH_2]; 2.2 [3H, CH_3] in ppm.

2-[(N-Benzyl-N-2-pyridylmethylamine)]-4-methyl-6-[N-(2-pyridylmethyl)aminomethyl)])-4-methyl-6-formylphenol (H_2BPPAMFF). To a solution of BPAPyFF (2.11 g, 4.8 mmol in 20 mL of CH_2Cl_2) was slowly added a solution of 2-chloromethyl-4-methyl-6-formylphenol (0.88 g, 4.8 mmol in 30 mL of CH_2Cl_2), under stirring. After the addition, the reaction was stirred for 24 h. The compound was washed with 5 × 30 mL of saturated aqueous Na_2CO_3 (pH 10), and the organic layer was dried over Na_2SO_4 and concentrated under a reduced pressure. A yellow solid was obtained. Yield: 70%. ^{1}H NMR δH (400 MHz; $CDCl_3$): 10.2 [1H, aldehyde]; 8.5 [2H, Py]; 7.6−6.8 [15H, Ar]; 3.8−3.6 [12H, CH_2]; 2.2 [6H, CH_3] in ppm. CHN% ($C_{37}H_{38}N_4O_3$) found (calcd.) C 75.2 (75.7), H 6.1 (6.5), N 9.5 (9.2); fp (57−62 °C).

*Synthesis of the Complex [Ni_2(HBPPAMFF)(μ-OAc)$_2$(H_2O)]BPh_4 (**1**).* Complex **1** was synthesized in methanolic solution by mixing $Ni(ClO_4)_2 \cdot 6H_2O$ (0.73 g, 2 mmol, in 20 mL) and the H_2BPPAMFF ligand (0.58 g, 1 mmol, in 20 mL) with stirring and mild heating (60 °C). After 15 min, $NaCH_3COO \cdot 3H_2O$ (0.16 g, 2 mmol) was added, and a green solution was obtained. $NaBPh_4$ (0.34 g, 1 mmol) was then added; immediately, a light green solid was formed, filtered off, and

dx.doi.org/10.1021/ic300018t | Inorg. Chem. 2012, 51, 6104−6115

Scheme 2. Synthesis of the Ligand H_2BPPAMFF

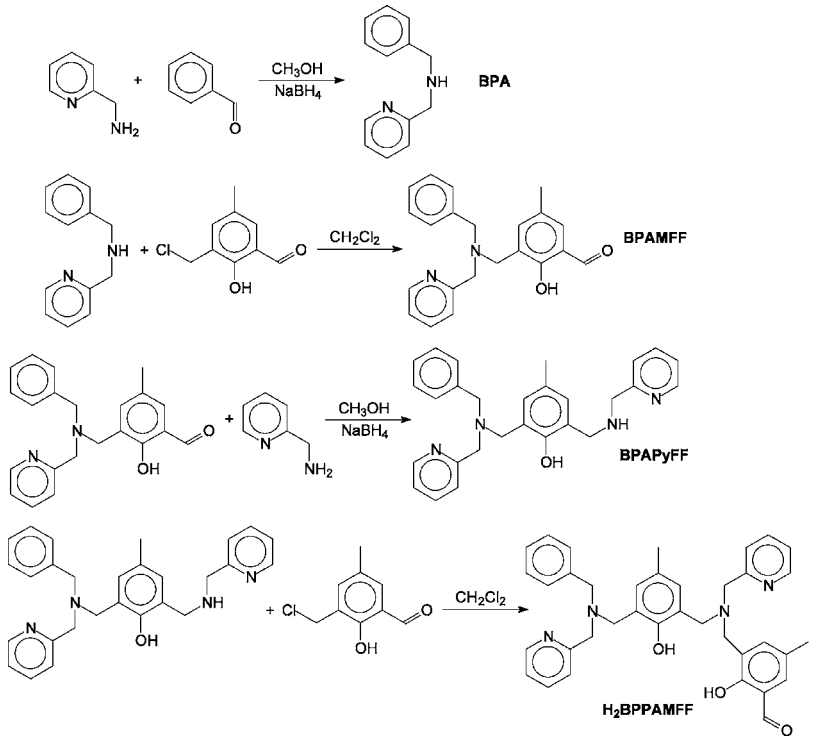

dried under vacuum for 24 h. Yield: 58%. IR (KBr), in cm^{-1}: ν(C−H_{Ar} and C−H_{Aliph}) 3431−2922; ν(BPh_4) 1606; ν_{ass}(OAc) 1554; ν_{sym}(OAc) 1427; ν(H−O_{phen}) 1317; ν (C−O) 1263; δ(C−H_{Ar}) 734 and 705. CHN% Calcd. for $Ni_2C_{65}H_{67}N_4O_8B$ (found): C 67.2 (67.6); H 5.8 (5.7) N 4.8 (4.9). Λ_M =120 $\Omega^{-1}\cdot cm^2\cdot mol^{-1}$ in CH_3CN electrolyte 1:1.

Caution! *Perchlorate salts with organic ligands are potentially explosive and must be handled in small amounts with care.*

*Synthesis of the Complex [Ni_2(HBPPAMFF)(μ-OBz)$_2$(H_2O)]ClO_4 (**1b**).* Complex **1b** was synthesized as described for complex **1** but with the use of sodium benzoate instead of sodium acetate. Suitable crystals for X-ray analysis were obtained after two weeks by slow diffusion of isopropanol in an acetonitrile solution of **1b**. It is important to mention here that the yield of this reaction is very low when compared to that of **1**, and thus, it was used only to fully characterize the structure of **1b** in which both Ni^{II} centers have similar coordination environments as those proposed for the μ-acetate complex **1**.

Synthesis of Silica Nanospheres (SiO_2). This preparation is a modification of the reverse microemulsion reported elsewhere.[39] In a 500 mL round-bottomed flask, 15.5 g of polyoxyethylene (5) nonylphenylether (IGEPAL CO-520, Aldrich Co.) was dissolved in 250 mL of cyclohexane. The mixture was sonicated for 3 min, and then, 2.75 mL of TEOS (tetraethylorthosilicate) and 5.4 mL of ammonium hydroxide solution (29%) were added. The reaction mixture was kept under magnetic stirring for 24 h. The material was then precipitated with methanol, collected by centrifugation (7000 rpm, 30 min), and washed 3 times with ethanol. The material was oven-dried at 100 °C.

*Preparation of Organoalkoxysilane and Immobilization of Complex **1** on SiO_2 Nanospheres (SiO_2-**1**).* (3-Aminopropyl)-triethoxysilane (APTES) (0.3 μL) was added to 3 mL of complex **1** solution (2.1×10^{-4} mol·L^{-1} in acetonitrile), corresponding to 1:1 amine/aldehyde molar ratios. The mixture was stirred at room temperature for 15 min in order to prepare the alkoxysilane of complex **1**. To the solution obtained above was added 100 mg of SiO_2 nanospheres. The reaction mixture was kept under magnetic stirring at room temperature for 24 h and then separated by centrifugation and washed three times with acetonitrile. The supernatant solution was stored quantitatively to determine the amount of complex **1** immobilized on the support by comparing the UV−vis absorption maximum near 400 nm for the alkoxysilane-complex solutions obtained before and after immobilization. Typically, the immobilization is quantitative, which corresponds to a complex **1** loading of 6×10^{-6} mol·g^{-1}

Reactivity Studies. Phosphatase-like activity of complex **1** was determined through the hydrolysis reaction of the model substrate bis(2,4-dinitrophenyl)phosphate [2,4-BDNPP] under substrate excess. The experiments were carried out in triplicate and spectrophotometrically monitored at 400 nm (ε = 12 100 L·$mol^{-1}\cdot cm^{-1}$) using a Varian Cary 50 BIO UV−Vis spectrophotometer coupled to a thermostat bath. Reactions were monitored to less than 5% conversion of 2,4-BDNPP to 2,4-DNP, and the data was treated using the initial rate method. Initial rates were obtained directly from the plot of the 2,4-dinitrophenolate concentration (2,4-DNP) versus time under the same experimental conditions. In these experiments, all of the solutions were prepared in aqueous/buffer media, except the complex stock solution (3.0×10^{-4} mol·L^{-1} in acetonitrile). Studies regarding the effects of pH on the hydrolysis reaction were performed in the pH range 5.00−10.5 (MES pH 4.00−6.50; HEPES pH 7.00−8.50; CHES pH 9.00−10.5; I = 0.1 mol·L^{-1} with $LiClO_4$), under a 100-fold excess of substrate, at 25 °C. Experiments to determine the dependence of the reaction rate on the substrate concentration were carried out at 25 °C and pH 9.00 for both substrates (2,4-BDNPP and 2,4-DNPP).

The heterogeneous reaction was performed under the same conditions as described above. The reactions were carried out in a 4 mL thermostatic glass reactor equipped with a magnetic stirrer. In a typical reaction employing the heterogeneous catalyst, SiO_2-**1** (2.2×10^{-8} mol) was weighed in a vial flask. The solid was suspended (0.15 mL of buffer and 0.14 mL of acetonitrile), and 0.1 mL of the substrate, 2,4-BDNPP, was added, resulting in a catalyst/substrate molar ratio of 1:100. The hydrolysis reaction was carried out during a controlled time interval (30 min) under magnetic stirring. The solution containing the reaction products was separated from the solid catalyst by centrifugation and analyzed by UV−vis. The same procedure was followed for the control reactions using the corresponding silica supports without the complex.

dx.doi.org/10.1021/ic300018t | *Inorg. Chem.* 2012, 51, 6104−6115

Scheme 3. Proposed Equilibria Observed for Complex 1 in Acetonitrile/Water (50:50) Solution

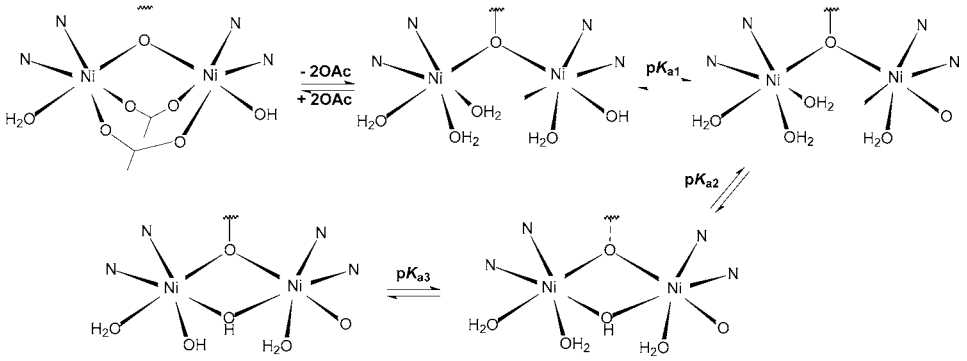

RESULTS AND DISCUSSION

Synthesis of the Ligand H_2BPPAMFF. Silica or other nanomaterials coated by silica can be easily reacted with 3-aminopropyltriethoxysilane (APTES) to generate amino-functionalized surfaces, and in this case, the design of a ligand with a free aldehyde group could be the best choice for binding the desired ligand or complex to the silica matrix via an imine bond. Alternatively, the ligand or complex can be first reacted with APTES (equimolar) to prepare an organoalkoxysilane that can easily react with silanol groups of silica surfaces. On the basis of the structures of the ligand HL1 and the biomimetic Ni^{II} complex with very interesting catalytic activities previously reported (Scheme 1),[27] a new ligand was designed containing similar functional groups and an additional free aldehyde group to allow the covalent linkage to amino-functionalized surfaces or amino-alkoxysilanes. This new ligand contains an aldehyde group sterically hindered to be part of the coordination sphere of the metal center, and therefore, after complexation with metal ions, it will remain free for anchoring the silica matrix. The step by step approach for the synthesis of the ligand is depicted in Scheme 2. The last step involves an alkylation reaction of a secondary amine with 2-chloromethyl-4-methyl-6-formylphenol which gives rise to the desired aldehyde group opposite to the coordinating groups in the hexadentate dinucleating ligand. The purity and structure of H_2BPPAMFF was confirmed by ^{1}H NMR and elemental analysis.

Synthesis and Characterization of $[Ni_2(HBPPAMFF)(\mu\text{-}OAc)_2(H_2O)]BPh_4$ (1) and $[Ni_2(HBPPAMFF)(\mu\text{-}OBz)_2(H_2O)]ClO_4$ (1b). The reaction of $Ni(ClO_4)_2{\cdot}6H_2O$ with the ligand H_2BPPAMFF in methanol in the presence of $NaCH_3COO{\cdot}3H_2O$ and $NaBPh_4$ affords complex **1** as a light green solid. The IR spectrum of **1** shows bands at $\nu_{ass}(COO^-)$ at 1554 cm^{-1} and $\nu_s(COO^-)$ at 1427 cm^{-1} indicating the coordination of a carboxylate group in a bridging mode (Δ = 127 cm^{-1}).[62] The terminal phenolic vibration (δO−H) observed in the free ligand in 1375 cm^{-1} was observed in the complex (1317 cm^{-1}) indicating that this group was not deprotonated (Figure S1, Supporting Information) in agreement with the X-ray structure of **1b**. Magnetic susceptibility data for the free complex **1**, collected as a function of temperature (4.5−300 K) at a constant magnetic field, reveal a weak antiferromagnetic coupling (J = −3.1 K), which is in agreement with a structure containing the $\{Ni^{II}(\mu\text{-phenoxo})(\mu\text{-}OAc)_2\}$ moiety (vide infra).[27]

The electronic spectrum of **1** measured in acetonitrile solution exhibits features at 308 nm (ε = 4300 $mol{\cdot}L^{-1}{\cdot}cm^{-1}$) and 390 nm ($\varepsilon$ = 4700 $mol{\cdot}L^{-1}{\cdot}cm^{-1}$), which can be attributed to pπ → dπ^* intraligand charge transfer, and 604 nm (ε = 20 $mol{\cdot}L^{-1}{\cdot}cm^{-1}$) d−d transition, respectively (Figure S2, Supporting Information).

Cyclic voltammograms were recorded in acetonitrile in the potential range −2.0 to 2.0 V versus Ag/AgCl, using $[TBA][(PF)_6]$ as supporting electrolyte. In the cyclic voltammograms for complex **1**, two nonreversible cathodic waves were observed at −1.27 and −1.64 V versus NHE, at 100 $mV{\cdot}s^{-1}$ (Figure S3, Supporting Information). These redox potentials can be attributed to the electron transfer processes $Ni^{II}Ni^{II} \rightarrow Ni^{II}Ni^{I}/Ni^{II}Ni^{I} \rightarrow Ni^{I}Ni^{I}$. Interestingly, the redox process observed at −1.27 V in **1** is in close agreement with the value observed for the $Fe^{II}Ni^{II}/Fe^{II}Ni^{II}$ redox couple (−1.41 V) in a dinuclear model complex in which the Ni^{II} center has a similar coordination environment as in **1**.[12] The nonreversibility of these processes is indicative of the instability of the totally reduced form in solution. Repetitive CV scans of **1** showed the maintenance of the CV curve profile with no significant decrease in either cathodic or anodic waves.

The measured molar conductivity of **1** in acetonitrile solution at 25 °C was 120 $S{\cdot}cm^2{\cdot}mol^{-1}$, which is characteristic of a 1:1 electrolyte.[63]

Potentiometric titration studies of **1** (water/acetonitrile, 50:50) showed the neutralization of 3 mol of KOH per mol of complex in the pH range 3−12. After fitting the data with the BEST7 program (Figure S4, Supporting Information), three protonation constants were obtained at 3.91, 6.19, and 9.75. The dissociation of the bridging carboxylate groups of **1** in aqueous medium is quite in line with its well-documented lability, which is facilitated by increasing the pH of the solution.[64,65]

These pK_a values are consistent with the following equilibria obtained for a similar dinuclear $Ni^{II}Ni^{II}$ complex without a coordinated terminal phenol/phenolate group:[27] complex **1** $[LH(OH_2)Ni^{II}(\mu\text{-}AcO)_2Ni^{II}(OH_2)] \leftrightarrow [L\text{-}(OH_2)_3Ni^{II}Ni^{II}(OH_2)] \leftrightarrow [L(OH_2)_2Ni^{II}(\mu{-}OH)Ni^{II}(OH_2)] \leftrightarrow [L(OH_2)(OH)Ni^{II}(\mu{-}OH)Ni^{II}(H_2O)]$, as shown in Scheme 3 ($H_2$BPPAMFF = H_2L). Thus, pK_{a1} is assigned to deprotonation of the coordinated phenol ligand (also observed in the crystal structure of complex **1b**), while pK_{a2} and pK_{a3} are, respectively, attributed to the formation of a $Ni^{II}(\mu{-}OH)Ni^{II}$ species and deprotonation of a Ni^{II}-bound water molecule, resulting in the catalytically active species (vide infra). In fact, this proposal is strongly supported by the ESI-MS data of **1** under kinetic experimental conditions (vide infra).

In order to obtain a crystal for structural characterization of complex **1**, we tried many different crystallization techniques such as changing counterions and exogenous bridging groups of complex **1**. Finally, we obtained a crystal suitable for X-ray

dx.doi.org/10.1021/ic300018t | Inorg. Chem. 2012, 51, 6104−6115

diffraction analysis of the di-μ-benzoate complex $[NiNi(HBPPAMFF)(\mu\text{-}OBz)_2(H_2O)]^+$ (**1b**). Complex **1b** crystallizes as green single crystals in acetonitrile/isopropanol diffusion that belong to the monoclinic crystal system and space group $P2_1/c$. An ORTEP view of the cation complex is presented in Figure 1.

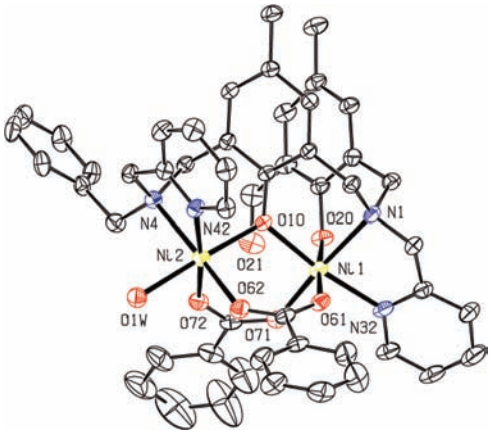

Figure 1. ORTEP view of $[NiNi(HBPPAMFF)(\mu\text{-}OBz)_2(H_2O)]^+$ (**1b**). Ellipsoids are drawn at 40% probability level. For clarity, only a partial labeling scheme is shown (Figure S5, Supporting Information, shows all atoms labeled).

The crystallographic data and the main bond distances/angles are given in Tables 1 and 2. The resolution of the crystal

Table 2. Selected Bond Lengths (Å) and Angles (deg) for Complex 1b

Ni1−Ni2	3.3968(12)	Ni2−O72	2.029(5)
Ni1−O10	1.997(4)	Ni2−O10	2.039(4)
Ni1−O71	2.022(5)	Ni2−O62	2.044(5)
Ni1−O61	2.028(5)	Ni2−N42	2.087(6)
Ni1−N32	2.068(6)	Ni2−O1W	2.089(5)
Ni1−N1	2.119(5)	Ni2−N4	2.184(5)
Ni1−O20	2.175(5)		
O10−Ni1−O71	96.55(19)	O72−Ni2−O62	94.8(2)
O10−Ni1−O61	93.02(18)	O10−Ni2−O62	94.18(18)
O71−Ni1−O61	100.2(2)	O72−Ni2−N42	173.2(2)
O10−Ni1−N32	171.5(2)	O10−Ni2−N42	92.02(19)
O71−Ni1−N32	91.9(2)	O62−Ni2−N42	91.5(2)
O61−Ni1−N32	86.5(2)	O72−Ni2−O1W	84.2(2)
O10−Ni1−N1	90.63(18)	O10−Ni2−O1W	174.52(19)
O71−Ni1−N1	165.8(2)	O62−Ni2−O1W	86.70(19)
O61−Ni1−N1	91.5(2)	N42−Ni2−O1W	93.4(2)
N32−Ni1−N1	80.9(2)	O72−Ni2−N4	93.15(19)
O10−Ni1−O20	91.72(17)	O10−Ni2−N4	91.07(17)
O71−Ni1−O20	79.54(19)	O62−Ni2−N4	170.5(2)
O61−Ni1−O20	175.25(19)	N42−Ni2−N4	80.42(19)
N32−Ni1−O20	88.8(2)	O1W−Ni2−N4	88.83(19)
N1−Ni1−O20	88.1(2)	Ni1−O10−Ni2	114.62(19)
O72−Ni2−O10	90.32(18)		

structure of **1b** shows an asymmetric unit composed of a cation complex $[Ni_2(HBPPAMFF)(\mu\text{-}OBz)_2(H_2O)]^+$ and a perchlorate anion as the counterion. Figure 1 shows the structure of the cation complex, which is composed of one unsymmetrical ligand H_2BPPAMFF coordinated to two Ni^{II} atoms (Ni1 and Ni2). Each Ni^{II} center is six coordinated and bridged by two exogenous benzoate groups coordinated in the bidentate mode and by the phenoxo endogenous bridge. Both Ni^{II} centers are in an N2O3 coordination environment arranged in distorted octahedral geometries, as evidenced by all of the angles around them that deviate from 180° and 90° (Table 2). The Ni1 center is bound to two nitrogen atoms [N1 (tertiary amine) and N32 (pyridine)] and by the terminal protonated O20 phenol oxygen, which are arranged in a facial mode and belong to the pendant arm of the binucleating ligand H_2BPPAMFF. It is important to note that the Ni1−O20 bond length (2.175(5) Å) is significantly longer compared to the $Ni-O_{phenolate}$ distances in other dinuclear $Ni^{II}Ni^{II}$ and mononuclear Ni^{II} complexes where the phenol group is deprotonated ($Ni-O_{phenolate}$ bond distances are in the range 1.97 to 2.00 Å).[66,67] In fact, in complex **1b**, the presence of the H atom on the terminal phenol leads to the weaker interaction between Ni1 and O20 (Ni1−O20 = 2.175 Å) than that between Ni1 and the bridging phenolate O10 (Ni1−O10 = 1.997 Å). Besides the nitrogen atoms, the coordination sphere of the Ni1 center is completed by three oxygen atoms, O61 and O71, provided by the exogenous benzoate bridges, and O10 from the endogenous phenoxo group. The coordination sphere of the Ni2 center is composed of the amine nitrogen N4, trans positioned to the oxygen atom O62, the nitrogen pyridine N42 trans to the oxygen O72, and the oxygen OW1 (from an water molecule) trans to the oxygen O10 (from an phenoxo bridge).

On the basis of the characterization of complex **1** by different techniques, the X-ray structure of complex **1b**, the similarity of H_2BPPAMFF to ligands reported previously in the literature,[27] and the ligand geometry that favors the coordination of two metal centers, complex **1** can be formulated as $[Ni_2(HBPPAMFF)(\mu\text{-}AcO)_2(H_2O)]BPh_4$ as shown in Figure 2.

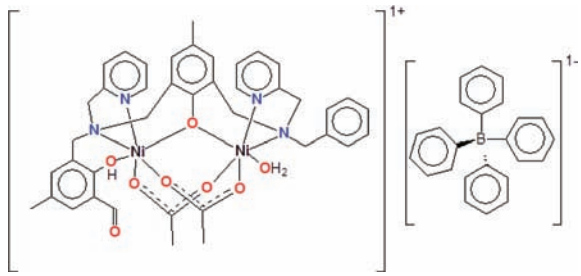

Figure 2. Proposed structure for complex **1**.

In order to establish unequivocally the catalytically relevant species for the hydrolysis of diester bonds, ESI-MS studies were carried out in CH_3CN/water solutions (50:50), the same solvent conditions as those employed for kinetic assays for complex **1**. Figure 3 shows the spectrum in CH_3CN/water, while Figure S6, Supporting Information, shows the observed and expected isotopic distribution for the assigned species under these experimental conditions. As can be observed in Figure 3, four main groups of peaks are observed at mass to charge (m/z) ratios of 865.20, 759.11, 643.20, and 359.00. The peak at m/z = 865.20 can be attributed to $[Ni_2LH(\mu\text{-}OAc)_2(C_2H_5OH)]^+$ (L= HBPPAMFF), which correspond to a cation similar to the complex **1b** shown in Figure 1 with acetate ions instead of benzoate ions and an ethanol molecule coordinated to the nickel center instead of water which may arise from reduction of acetate in the ion spray. The next group of peaks at m/z = 759.11 is best interpreted in terms of a dinuclear nickel complex with one μ−OH group and one

dx.doi.org/10.1021/ic300018t | Inorg. Chem. 2012, 51, 6104−6115

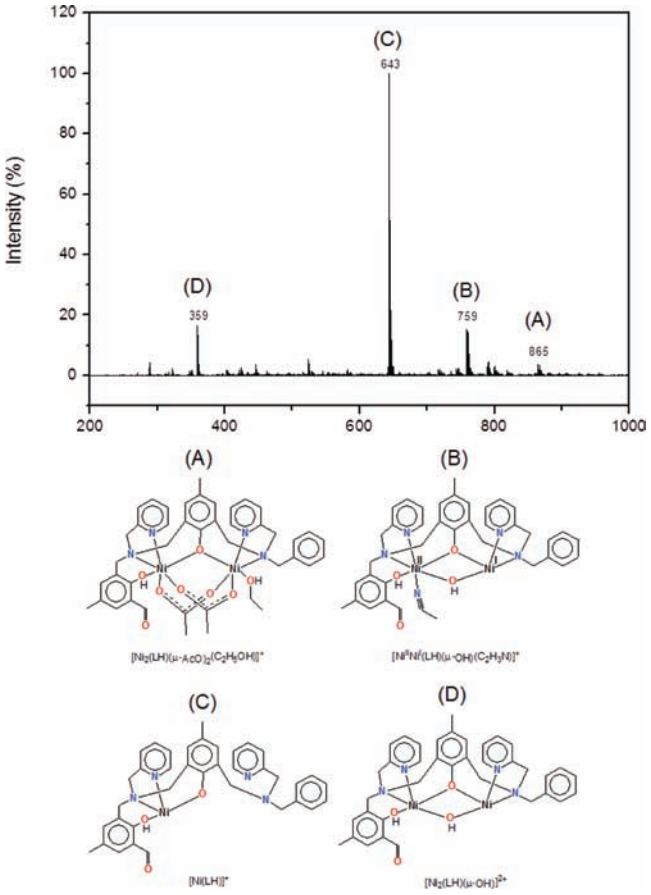

Figure 3. ESI-MS analysis of complex **1** CH_3CN/water solutions (50:50).

CH_3CN ligand ($[Ni^{II}Ni^{I}HL(\mu\text{-}OH)(CH_3CN)]^+$), indicating reduction of the Ni^{II} center coordinated by the soft side of the ligand ion under the conditions of the eletrospray ionization (see electrochemistry), while the group of peaks at 359.08 is likely due to the dication $[Ni_2HL(\mu\text{-}OH)]^{2+}$ without exogenous ligands (i.e., carboxylate, H_2O, CH_3CN, or C_2H_5OH). Finally, the major peak at 643.22 can be assigned to the mononuclear $[NiHL]^+$ species in which the ligand does not undergo fragmentation but one nickel atom, most probably from the bidentate side of the ligand, becomes dissociated from the dinuclear complex under the conditions of the eletrospray ionization. It is important to emphasize that the dinuclear species $[Ni_2HL(\mu\text{-}OH)(CH_3CN)]^+$ and $[Ni_2HL(\mu\text{-}OH)]^{2+}$ identified from the ESI-MS experiments corroborate very well with the proposed protonation/deprotonation equilibrium from potentiometric titration (vide supra).

Immobilization of Complex 1 on Silica Nanospheres. The silica nanospheres used in this study were prepared by means of a reverse microemulsion formulation with cyclohexane and a nonionic surfactant. The reverse microemulsion is an isotropic and thermodynamically stable single-phase that consists of water nanodroplets stabilized by the surfactant molecules and dispersed in the oil phase. The nanodroplets serve as nanoreactors for the synthesis of the silica nanospheres of controlled size. The silica matrix is formed by hydrolysis and condensation of TEOS by adding ammonium hydroxide to the reverse microemulsion phase. The transmission electron microscopy (TEM) analysis of the samples reveals nearly spherical particles of ca. 32 nm (Figure S7, Supporting Information).

The strategy for the immobilization of complex **1** in the silica nanospheres consists in the modification of complex **1** with (3-aminopropyl)triethoxysilane (APTES) followed by reaction of the alkoxysilane-complex formed in situ with the silica nanospheres. The color of the solution containing the complex changed from light green to yellow, and after centrifugation and washing, the silica matrix ended up becoming yellow. The IR spectrum of SiO_2-**1** contains broad and strong vibrational bands of Si−OH, Si−O, and Si−O−Si typical of amorphous silica that overlay the features corresponding to complex **1** (Figure S8, Supporting Information). Therefore, we discuss the IR spectrum in terms of the free ligand compared to the alkoxysilane-modified ligand formed by reacting the ligand H_2BPPAMFF and APTES. After reaction with APTES, the IR spectrum is characterized by the disappearance of the carbonyl band at 1679 cm^{-1} (νC═O) of the aldehyde group and the appearance of a new band at 1630 cm^{-1} (νC═N), which is a strong indication of the formation of the imine bond (Figure 4). The electronic spectrum of the alkoxysilane-modified ligand

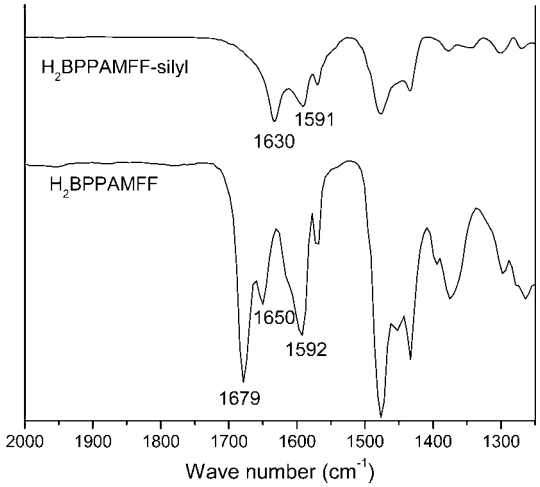

Figure 4. IR spectra of the ligand H_2BPPAMFF and the alkoxysilane-modified ligand in solid state (KBr pallet) in the range from 1250 to 2000 cm^{-1}. IR spectra in the full range from 400 to 4000 cm^{-1} are shown in Figure S9, Supporting Information.

exhibits a strong absorption at 420 nm, absent in the H_2BPPAMFF ligand, which can also be attributed to the formation of the imine bond (Figure 5c). These results confirmed the silylation of the ligand, and since the alkoxysilane groups are likely to hydrolyze and condensate with the silanol groups on silica surfaces, we can conclude that the ligand was properly modified to be covalently attached to silica spheres.

After immobilization of complex **1**, the color of silica changed to that characteristic of complex **1**. The electronic spectrum of SiO_2-**1**, measured in solid state (KBr pellets), exhibits features at 380, 415, and 560 nm (Figure 5d). The absorption band at 415 nm can be attributed to the immobilization of complex **1** with the formation of imine bond, also observed in the alkoxysilane-ligand (Figure 5c), while the broad band centered at 560 nm can be assigned to d−d transitions. The spectrum of the pure complex **1** (Figure 5b) in CH_3CN solution shows the corresponding transition at 604 nm, which clearly indicates that the coordination environment around the Ni^{II} centers is affected when complex **1** is anchored

dx.doi.org/10.1021/ic300018t | Inorg. Chem. 2012, 51, 6104−6115

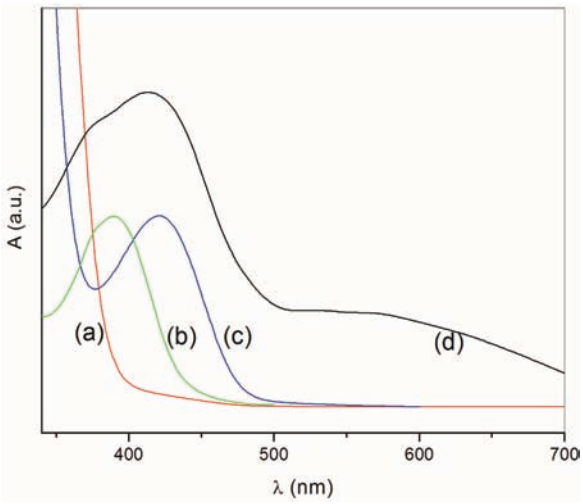

Figure 5. UV−vis spectra of (a) H_2BPPAMFF ligand, (b) complex **1**, (c) alkoxysilane-ligand in acetonitrile solution, and (d) SiO_2-**1** in solid state (KBr pellet).

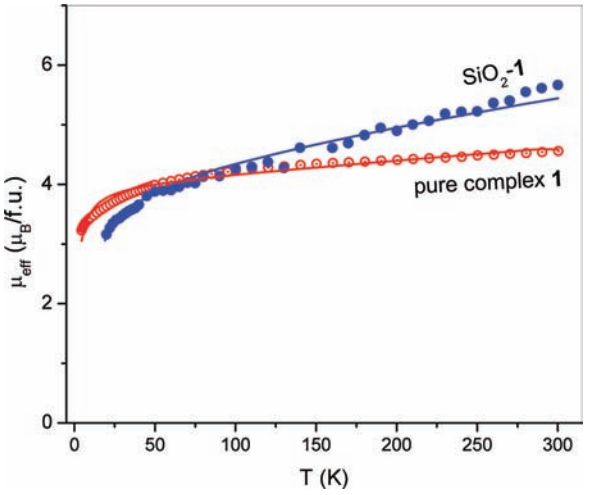

Figure 6. Temperature dependence of the effective magnetic moment for complex **1** (open circle) and its contribution extracted from SiO_2-**1** (solid circle). Solid lines are fits (see text).

to SiO_2. From this information, it seems reasonable to assume that in SiO_2-**1**, the acetate bridging ligands are replaced by solvent molecules, most probably with the formation of a [Ni(μ−OH)Ni] structural unit. In fact, this interpretation is quite in line with the magnetic results of **1** and SiO_2-**1** (vide infra).

In order to follow possible structural modifications when complex **1** is anchored to silica nanospheres (SiO_2-**1**), magnetic measurements were carried out. The raw magnetic data showed paramagnetism of the pure dinuclear Ni^{II} complex **1** in the whole temperature range and diamagnetism of SiO_2 and SiO_2-**1** in the temperature range above 6 and 15 K, respectively. While the crossover to paramagnetism for SiO_2-**1** composite is expected, for SiO_2 it probably results from the presence of a small amount of impurity of unknown origin. In order to obtain the magnetic contribution of the dinuclear Ni^{II} complex **1** in the SiO_2-**1** composite, magnetic contribution of SiO_2 was subtracted. This was taken as the susceptibility of the separately measured SiO_2 compound.

In Figure 6, the temperature dependence of the effective magnetic moment (μ_{eff} = 2.828 $(\chi_{mol}T)^{1/2}$) is shown for the pure dinuclear complex **1**, and for the corresponding magnetic contribution extracted from the SiO_2-**1** composite.

The data in Figure 6 were fitted to the Hamiltonian given in eq 1

$$\hat{H} = -JS_1S_2 + \Sigma_i D_i S_i^2 + \Sigma_i g\mu_B HS_i \quad i = 1, 2 \qquad (1)$$

where J is the magnetic exchange constant, $S_1 = S_2$ is the spin of the Ni^{II} ion, equal to 1, D is the zero field splitting parameter, g the spectroscopic factor, H is the magnetic field, and μ_B is the Bohr magneton. The parameters obtained from the fits are J = −3.1 ± 2 K, g = 1.97 ± 0.03, D = 0, and TIP = (2485 ± 800) × 10^{-6} emu·mol^{-1} for the pure complex **1**; J = −14.8 ± 3 K, g = 1.97 ± 0.03, D = 0, and TIP = (6101 ± 900) × 10^{-6} emu·mol^{-1} for extracted complex **1**, where TIP means temperature independent paramagnetism. D was put equal to zero in order to avoid overparametrization.

In fact, the weak antiferromagnetic coupling (J = −3.1 K) obtained for the pure complex **1** is in agreement with a structure containing the {Ni^{II}(μ-phenoxo)(μ-OAc)$_2$} moiety in which the magnetic interaction generally varies from anti-ferromagnetism to ferromagnetism on introducing slight changes in the dinuclear core.[27]

The essential difference between complex **1** and SiO_2-**1** lies in the J and TIP parameters. As can be observed, both are greater for the dinuclear Ni^{II}-complex anchored to SiO_2-**1**. The stronger antiferromagnetic coupling in the anchored complex SiO_2-**1** probably originates due to the formation of a Ni^{II}(μ−OH)Ni^{II} moiety, which in principle should approximate the Ni^{II} centers, given rise to a more effective overlapping of the d-metal and bridging oxygen orbitals, thus increasing the interchange coupling.[68] However, it should be noted that such an interpretation is merely speculative, given that no structural information are available for the SiO_2-**1** anchored system. The TIP parameters are too large and may result from some parasitic effects, which have not been taken into account, such as impurity contained in SiO_2 but not present in the SiO_2-**1** composite. In summary, the magnetic results clearly confirm that the dinuclear Ni^{II} complex was anchored to the silica nanospheres and that the coordination geometry around the Ni^{II} centers is somewhat modified with respect to the pure complex **1**. Indeed, the kinetic data obtained from the hydrolysis reaction of the diester phosphate 2,4-BDNPP catalyzed by **1** and SiO_2-**1** are in full agreement with this hypothesis (vide infra).

Reactivity Studies. The catalytic activity of complex **1** immobilized in silica nanospheres (SiO_2-**1**) in the cleavage of 2,4-BDNPP is strongly influenced by the pH of the reaction mixture. The pH/rate profile curve shown in Figure 7a was fitted using a Boltzman model to give a pK_a value of 8.0, which can be attributed to deprotonation of a Ni^{II}-bound water molecule to generate the catalytically active species [(OH)Ni-(μ−OH)Ni(OH_2)] when **1** is linked to silica.[69]

The catalytic activity of complex **1** in the cleavage of 2,4-BDNPP is also strongly influenced by the pH of the reaction mixture with an exponential growth pH/rate profile (Figure 7b). However, as expected, for the reaction catalyzed by the free complex **1**, no fully sigmoidal curve could be obtained since the pK_a = 9.75 (see potentiometric titration) to generate the catalytically active species [(OH)Ni(μ−OH)Ni(OH_2)] lies in the higher end of the investigated pH range. Thus, for both reactions, these results strongly suggest that the rate of the catalytic reaction depends on the deprotonation of the Ni^{II}

dx.doi.org/10.1021/ic300018t | Inorg. Chem. 2012, 51, 6104−6115

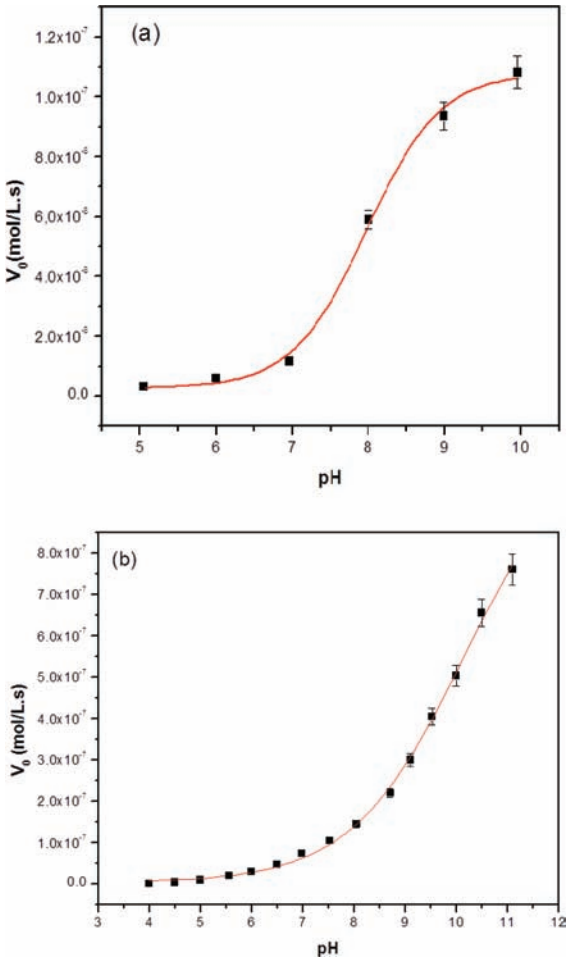

Figure 7. Dependence of the initial reaction rate (V_0) on pH for the hydrolysis of 2,4-BDNPP promoted by SiO_2-**1** (a) and complex **1** (b). Conditions: [complex] = 1.0×10^{-5} mol·L^{-1}; [2,4-BDNPP] = 1.0×10^{-3} mol·L^{-1}; [buffers] = 50×10^{-3} mol·L^{-1}; I = 50×10^{-3} mol·L^{-1} ($LiClO_4$) in H_2O/CH_3CN (50% v/v) at 25 °C.

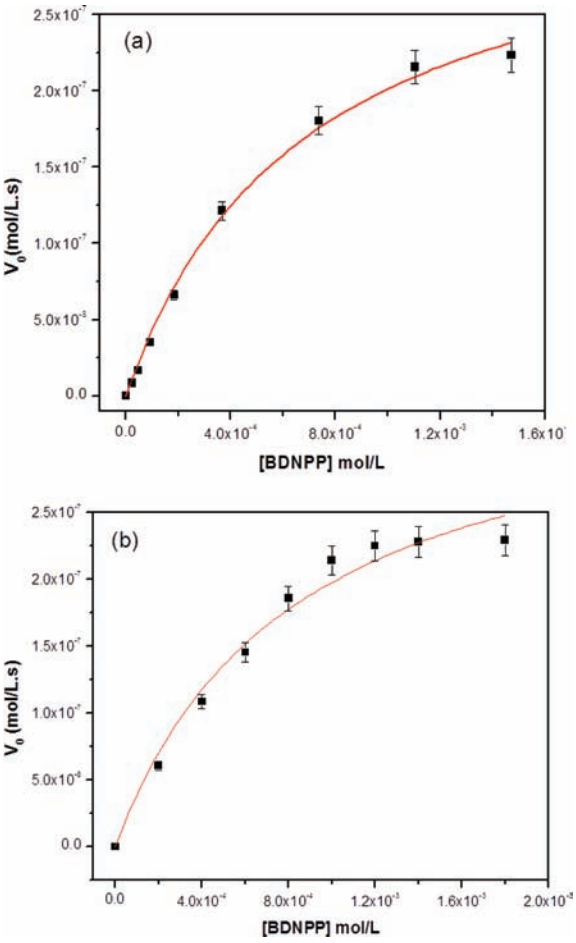

Figure 8. Dependence of the initial reaction rate (V_0) on the 2,4-BDNPP concentration for the hydrolysis reaction promoted by SiO_2-**1** (a) and complex **1** (b). Conditions: [complex] = 1.0×10^{-5} mol·L^{-1}; [buffer] = 50×10^{-3} mol·L^{-1} (CHES, pH) 9.00; I = 50×10^{-3} mol·L^{-1} ($LiClO_4$) in H_2O/CH_3CN (50% v/v) at 25 °C.

coordinated water molecule of the catalytically active species of the type [(OH)Ni(μ−OH)Ni(OH$_2$)], as previously suggested for the Ni^{II}Ni^{II} analogues.[27,70,71] In fact, the distinct pK_a values observed for the pure complex **1** (potentiometic titration) and the anchored SiO_2-**1** system are in full agreement with the magnetochemical results, which clearly reveal that the coordination geometry around the Ni^{II} centers is somewhat modified when **1** is anchored to the silica nanospheres.

The dependence of the initial rates at pH 9.0 on the concentration of the substrate (0.2−1.8 mmol·L^{-1}) reveals saturation kinetics with Michaelis−Menten-like behavior (Figure 8). The kinetic parameters were obtained from nonlinear square fits using the program Origin 8.0 and the parameters V_0, K_M, and k_{cat} are shown in Table 3. BDNPP bound to free complex **1** hydrolyzes 138,400 times faster than free BDNPP (k_{uncat} = 3.88×10^{-7} s^{-1}) under identical experimental conditions,[59] while complex **1** immobilized in silica nanospheres hydrolyzes 2,4-BDNPP 118,500 times faster than the noncatalyzed reaction. The kinetic parameters K_{ass} (K_{ass} = 1/K_M in Table 3) reveal a higher stabilization of the substrate−catalyst intermediate for the heterogeneous reaction than for the reaction in homogeneous media (K_{ass} is about 2 times higher for SiO_2-**1**), while the catalytic turnover constant k_{cat} is slightly lower for the heterogeneous reactions ($k_{cathetero}$/$k_{cathomo}$ is about 0.85 for SiO_2-**1**). Nevertheless, considering the second order rate constant (E = k_{cat}/K_M), a distinct catalytic efficiency with E_{hetero}/E_{homo} of 2 can be observed for SiO_2-**1**, thus indicating that the heterogeneous system is more efficient than the soluble catalyst. The higher affinity of 2,4-BDNPP for the anchored system SiO_2-**1** presumably originates from some influence of the solid support. Particularly, for SiO_2-**1**, the stabilization may occur via interaction with the surface silanol groups.

However, $k_{cat} \cong 3.0 \times 10^{-3}$ s^{-1}, obtained for the hydrolysis of 2,4-BDNPP by SiO_2-**1** at pH = 7.0, lies in the range of values (4.0×10^{-4} to 3.0×10^{-3} s^{-1}) found for a series of mixed-valence [Fe^{III}M^{II}] complexes (M^{II} = Fe, Mn, Co, Ni, Cd) with the same substrate.[10,38,58] In addition, it is important to emphasize here that, besides its catalytic activity, the anchored SiO_2-**1** system has the advantage that it can be reused with similar efficiency for subsequent diester hydrolysis reactions.

In order to assess the possible hydrolysis of the monoester 2,4-DNPP, one of the products formed from the hydrolysis reaction of the diester 2,4-BDNPP, a stoichiometric reaction between complex **1** and the 2,4-DNPP substrate, was monitored. It was observed that 2 equiv of 2,4-DNPP is released in 12 h for complex **1** at 25 °C, which indicates the hydrolysis of both the mono- and diester. On the basis of this information and assuming that the hydrolysis reaction of the

dx.doi.org/10.1021/ic300018t | Inorg. Chem. 2012, 51, 6104−6115

Table 3. Kinetic Parameters for the 2,4-BDNPP Hydrolysis Promoted by Free and Immobilized Complex 1 at 25 °C and pH 9.0

	V_0 (mol·L·s^{-1})	K_M (mol·L^{-1})	k_{cat} (s^{-1})	K_{ass} (L·mol^{-1})[a]	E (L·s^{-1}·mol^{-1})[b]	f[c]	turnover (h^{-1})
1	5.37×10^{-7}	1.57×10^{-3}	5.37×10^{-2}	637	34.2	138,400	33.4
SiO_2-**1**	3.40×10^{-7}	6.90×10^{-4}	4.6×10^{-2}	1450	66	118,500	32.7
1-2,4-DNPP	2.04×10^{-9}	3.0×10^{-5}	2.04×10^{-3}	33,333	68	105	

[a] $K_{ass} = 1/K_M$. [b] $E = k_{cat}/K_M$ (catalytic efficiency). [c] $f = (k_{cat}/k_{uncat})$; $k_{uncat} = 3.88 \times 10^{-7}$ s^{-1}.

2,4-BDNPP diester leads to the formation of an intermediate (presumably the monoester coordinated to the catalyst), we decided to investigate the catalytic activity of complex **1** in the hydrolysis of the monoester 2,4-DNPP. As can be observed in Figure 9, the initial rates as a function of substrate

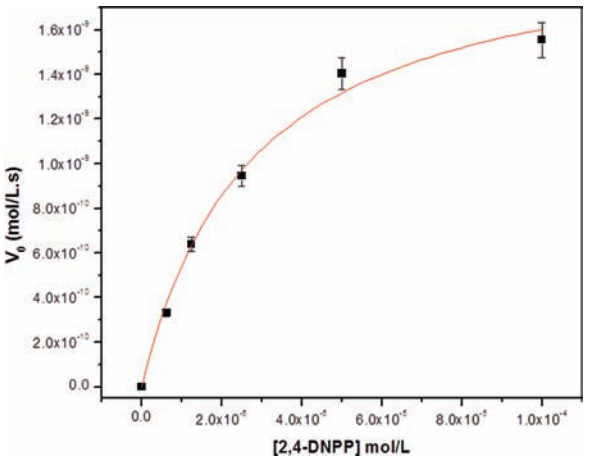

Figure 9. Dependence of the initial reaction rate (V_0) on the 2,4-DNPP concentration for the hydrolysis reaction promoted by complex **1**. Conditions: [complex] = 1.0×10^{-6} mol·L^{-1}; [buffer] = 50×10^{-3} mol·L^{-1} (CHES, pH) 9.00; $I = 50 \times 10^{-3}$ mol·L^{-1} ($LiClO_4$) in H_2O/CH_3CN (50% v/v) at 25 °C.

concentration reveal saturation kinetics with Michaelis–Menten-like behavior. The kinetic parameters, $k_{cat} = 2.04 \times 10^{-3}$ s^{-1} and $K_{ass} = 33{,}333$ mol^{-1}·L reveal that the association constant of the monoester with catalyst **1** is about 52 times greater, while k_{cat} is 26 times lower when compared to those parameters obtained with the corresponding 2,4-BDNPP diester. These data allowed us to conclude that distinct nucleophile groups within complex **1** are acting as the catalysts in the hydrolysis of the mono- and diester-phosphate substrates. It is important to note that the spontaneous hydrolysis of the monoester 2,4-DNPP is about 50 times greater than the hydrolysis of the diester 2,4-BDNPP under similar experimental conditions.[59] Here, as observed for a similar dinuclear $Ni^{II}Ni^{II}$ complex,[27] the opposite is observed, clearly indicating that the hydrolysis reaction of the monoester is occurring through the attack of a poorer nucleophile than that responsible for the catalysis of the diester (Scheme 4).[72]

In order to establish whether the nucleophilic attack on the phosphorus atom was via the terminal hydroxide ion or a general base catalysis, isotopic effect was evaluated in the hydrolysis of 2,4-BDNPP in D_2O catalyzed by complex **1** and SiO_2-**1**. According to Burstyn and co-workers,[73] if $0.80 < (k_H/k_D) < 1.50$, this is indicative that there is no proton transference involved in the reaction limiting step, and suggests an intramolecular nucleophilic attack mechanism.[74] The k_H/k_D ratios obtained for complex **1** and SiO_2-**1** were all close to 0.95, which corroborate the presence of a hydrolysis reaction

Scheme 4. Proposed Mechanism for the Hydrolysis of 2,4-BDNPP Promoted by Complex 1

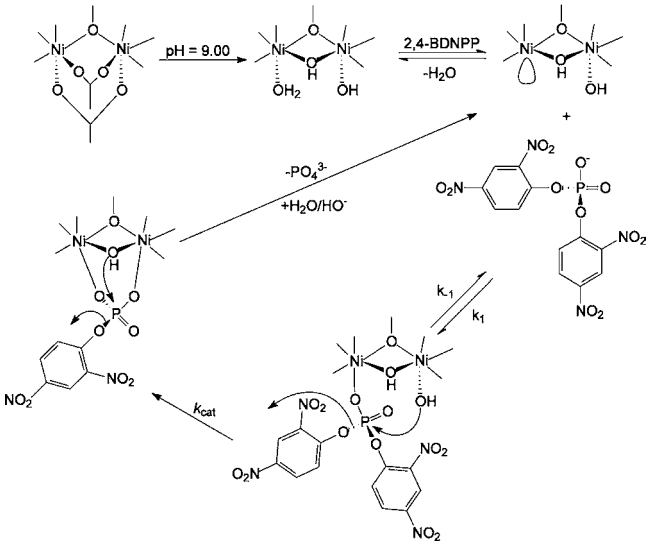

proceeding through an intramolecular mechanism, in which the phosphorus atom undergoes a nucleophilic attack promoted by the coordinated hydroxide ion.

The efficiency of immobilization of complex **1** without using APTES, which means by noncovalent bonding, is very low. Moreover, no significant rates of hydrolysis of 2,4-BDNPP were observed, when compared with uncatalyzed reaction. This suggests that the immobilization process by adsorption and most probably electrostatic bonds contributes to blocking the catalytic metal centers, which can be partially occupied by interaction with silica and less accessible to the substrate. The immobilization process by covalent bonding through imine bond formation reported here is more specific and allowed the interaction of the complex with the substrate to generate the active catalytic species to perform phosphatase-like activity with high turnover rates in the hydrolysis of 2,4-BDNPP. Finally, the SiO_2-**1** catalyst was reused in subsequent hydrolysis of 2,4-BDNPP, after washing the material in a Soxhlet extractor with 1:1 HEPES buffer pH 7/acetonitrile, and the rate of reaction was similar to that obtained in the first cycle. Therefore, it can be concluded that the SiO_2-**1** catalyst is stable for prolonged periods at least under the experimental conditions employed in the hydrolysis reactions.

■ CONCLUSIONS

In summary, a synthetic dinuclear Ni^{II} hydrolase, which contains a carbonyl group located in the ortho position of the terminal Ni^{II}-bound phenolate ligand, was covalently linked to silica using APTES. The complex attached to the solid surface of the nanomaterials maintained its phosphatase-like activity with high turnover rates in the hydrolysis of 2,4-BDNPP and catalytic rates as high as 118,500 times that of the uncatalyzed reaction. The heterogeneous system presented

dx.doi.org/10.1021/ic300018t | Inorg. Chem. 2012, 51, 6104–6115

higher catalytic efficiency (2 times that of the soluble complex), besides the higher complex to substrate association constant. Further studies of the complexes **1** and SiO_2-**1** on the activity of DNA hydrolysis to generate new possible drugs for technological applications, e.g, as anticancer agents, are underway and will be presented in future reports.

■ ASSOCIATED CONTENT

Supporting Information

X-ray crystallographic file in CIF format; Figures S1−S9 and Table S1 in PDF format. This material is available free of charge via the Internet at http://pubs.acs.org. Full tables of crystallographic data of complex **1b** (except structure factors) were deposited at Cambridge Structural Database (CCDC 843653), and these data are available free of charge from CCDC, 12 Union Road, Cambridge, CB2 1EZ, U.K. (fax, +44-1223-336-003; e-mail, deposit@ccdc.cam.ac.uk or http://www.ccdc.cam.ac.uk).

■ AUTHOR INFORMATION

Corresponding Author

*E-mail: ademir@qmc.ufsc.br (A.N.); lrossi@iq.usp.br (L.M.R.).

Notes

The authors declare no competing financial interest.

■ ACKNOWLEDGMENTS

We are grateful for grants that helped to support this research: CNPq, FAPESC, FAPESP, and INCT-Catalise (Brazil), BMBF/IB-BRA 07/2007 (Germany). We also thank Professor Pedro K. Kiyohara (IF-USP) for TEM analysis.

■ REFERENCES

(1) Liu, C.; Wang, M.; Zhang, T.; Sun, H. *Coord. Chem. Rev.* **2004**, *248*, 147.
(2) Mitic, N.; Smith, S. J.; Neves, A.; Guddat, L. W.; Gahan, L. R.; Schenk, G. *Chem. Rev.* **2006**, *106*, 3338.
(3) Strater, N.; Lipscomb, W. N.; Klabunde, T.; Krebs, B. *Angew. Chem.* **1996**, *35*, 2024.
(4) Sigman, D. S.; Mazumder, A.; Perrin, D. M. *Chem. Rev.* **1993**, *93*, 2295.
(5) Neves, A.; Rossi, L. M.; Horn, A., Jr.; Vencato, I.; Bortoluzzi, A. J.; Zucco, C.; Mangrich, A. S. *Inorg. Chem. Commun.* **1999**, *2*, 334.
(6) Neves, A.; Brito, M. A.; Drago, V.; Griesar, K.; Haase, W. *Inorg. Chim. Acta* **1995**, *237*, 131.
(7) Neves, A.; Brito, M. A.; Vencato, I.; Drago, V.; Griesar, K.; Haase, W. *Inorg. Chem.* **1996**, *35*, 2360.
(8) Neves, A.; Rossi, L. M.; Vencato, I.; Haase, W.; Werner, R. *Dalton Trans.* **2000**, *5*, 707.
(9) Neves, A.; Rossi, L. M.; Bortoluzzi, A.; Szpoganicz, B.; Schwingel, E.; Haase, W.; Ostrovski, S. *Inorg. Chem.* **2002**, *41*, 1788.
(10) Xavier, F. R.; Neves, A.; Casellato, A.; Peralta, R. A.; Bortoluzzi, A. J.; Szpoganicz, B.; Severino, P. C.; Terenzi, H.; Tomkowicz, Z.; Ostrovsky, S.; Haase, W.; Ozarowski, A.; Krzystek, J.; Telser, J.; Schenk, G.; Gahan, L. R. *Inorg. Chem.* **2009**, *48*, 7905.
(11) Franzoi, A. C.; Peralta, R. A.; Neves, A.; Vieira, I. C. *Talanta* **2009**, *78*, 221.
(12) Schenk, G.; Peralta, R. A.; Batista, S. C.; Bortoluzzi, A. J.; Szpoganicz, B.; Dick, A. K.; Herrald, P.; Hanson, G. R.; Szilagyi, R. K.; Riley, M. J.; Gahan, L. R.; Neves, A. *J. Biol. Inorg. Chem.* **2008**, *13*, 139.
(13) Hegg, E. L.; Burstyn, J. N. *Coord. Chem. Rev.* **1998**, *173*, 133.
(14) Piovezan, C.; Lisboa, F.; Castro, K. A. D. F.; Nunes, F. S.; Nakagaki, S.; Drechsel, S. M. *Appl. Catal., A* **2005**, *293*, 97.
(15) Guilherme, L. R.; Drechsel, S. M.; Tavares, F.; Cunha, C. J.; Castaman, S. T.; Nakagaki, S.; Vencato, I.; Bortoluzzi, A. J. *J. Mol. Catal. A: Chem.* **2007**, *269*, 22.
(16) Zhang, W. F.; Chen, X. G.; Li, P. W.; He, Q. Z.; Zhou, H. Y. *J. Appl. Polym. Sci.* **2007**, *103*, 1183.
(17) Terao, K.; Nakata, D.; Fukumi, H.; Schmid, G.; Arima, H.; Hirayama, F.; Uekama, K. *Nutr. Res.* **2006**, *26*, 503.
(18) Mura, P.; Corti, G.; Maestrelli, F.; Cirri, M. *J. Pharm. Biomed. Anal.* **2007**, *45*, 480.
(19) Vieira, A. P. D. A.; Da Silva, M. A. P.; Langone, M. A. P. *Lat. Am. Appl. Res.* **2006**, *36*, 283.
(20) Orcaire, O.; Buisson, P.; Pierre, A. C. *J. Mol. Catal. B: Enzym.* **2006**, *42*, 106.
(21) Chen, X. R.; Ju, Y. H.; Mou, C. Y. *J. Phys. Chem. C* **2007**, *111*, 18731.
(22) Fruhwirth, G. O.; Paar, A.; Gudelj, M.; Cavaco-Paulo, A.; Robra, K. H.; Gubitz, G. M. *Appl. Microbiol. Biotechnol.* **2002**, *60*, 313.
(23) Zucca, P.; Mocci, G.; Rescigno, A.; Sanjust, E. *J. Mol. Catal. A: Chem.* **2007**, *278*, 220.
(24) Salem, I. A. *Transition Met. Chem.* **2000**, *25*, 599.
(25) Halma, M.; Wypych, F.; Drechsel, S. M.; Nakagaki, S. *J. Porphyrins Phthalocyanines* **2002**, *6*, 502.
(26) (a) Bedioiu, F. *Coord. Chem. Rev.* **1995**, *144*, 39. (b) Bedioiu, F.; Devynck, J.; Bied-Charrenton, C. *Acc. Chem. Res.* **1995**, *28*, 30. (c) Barloy, L.; Lallier, J. P.; Battioni, P.; Mansuy, D.; Piffard, Y.; Tournoux, M.; Jones, W. *New J. Chem.* **1998**, *8*, 901.
(27) Greatti, A.; Scarpellini, M.; Peralta, R. A.; Casellato, A.; Bortoluzzi, A. J.; Xavier, F. R.; Jovito, R.; de Brito, M. A.; Szpoganicz, B.; Tomkowicz, Z.; Rams, M.; Haase, W.; Neves, A. *Inorg. Chem.* **2008**, *47*, 1107.
(28) Zhao, X.; Bagwe, R. P.; Tan, W. *Adv. Mater.* **2004**, *16*, 173.
(29) Bagwe, R. P.; Yang, C.; Hilliard, L. R.; Tan, W. *Langmuir* **2004**, *20*, 8336.
(30) Silva, P. R.; Vono, L. L. R.; Espósito, B. P.; Baptista, M. S.; Rossi, L. M. *Phys. Chem. Chem. Phys.* **2011**, *13*, 14946.
(31) Roy, I.; Ohulchanskyy, T. Y.; Pudavar, H. E.; Bergey, E. J.; Oseroff, A. R.; Morgan, J.; Dougherty, T. J.; Prasad, P. N. *J. Am. Chem. Soc.* **2003**, *125*, 7860.
(32) Tang, W.; Xu, H.; Kopelman, R.; Philbert, M. A. *Photochem. Photobiol.* **2005**, *81*, 242.
(33) Rossi, L. M.; Shi, L.; Quina, F. H.; Rosenzweig, Z. *Langmuir* **2005**, *21*, 4277.
(34) Azioune, A.; Slimane, A. B.; Hamou, L. A.; Pleuvy, A.; Chehimi, M. M.; Perruchot, C.; Armes, S. P. *Langmuir* **2004**, *20*, 3350.
(35) Qhobosheane, M.; Santra, S.; Zhang, P.; Tan, W. *Analyst* **2001**, *126*, 1274.
(36) Wang, Y.; Caruso, F. *Chem. Commun.* **2004**, *13*, 1528.
(37) Qin, F.; Zhou, Y. C.; Shi, J. L. *J. Biomed. Mater. Res., Part A* **2009**, *90A*, 333.
(38) Piovezan, C.; Jovito, R.; Bortoluzzi, A. J.; Terenzi, H.; Fischer, F. L.; Severino, P. C.; Pich, C. T.; Azzolini, G. G.; Peralta, R. A.; Rossi, L. M.; Neves, A. *Inorg. Chem.* **2010**, *49*, 2580.
(39) Jacinto, M. J.; Kioyhara, P. K.; Masunaga, S. H.; Jardim, R. F.; Rossi, L. M. *Appl. Catal., A* **2008**, *338*, 52.
(40) Philipse, A. P.; van Bruggen, M. P. B.; Pathmamanoharan, C. *Langmuir* **1994**, *10*, 92.
(41) Lu, Y.; Yin, Y.; Mayers, B. T.; Xia, Y. *Nano Lett.* **2002**, *2*, 183.
(42) Tada, D. B.; Vono, L. L. R.; Duarte, E. L.; Itri, R.; Kiyohara, P. K.; Baptista, M. S.; Rossi, L. M. *Langmuir* **2007**, *23*, 8194.
(43) Kobayashi, Y.; Horie, M.; Konno, M.; Rodriguez-Gonzalez, B.; Liz-Marzan, L. M. *J. Phys. Chem. B* **2003**, *107*, 7420.
(44) Lu, Y.; Yin, Y.; Li, Z. Y.; Xia, Y. *Nano Lett.* **2002**, *2*, 785.
(45) Kobayashi, Y.; Katakami, H.; Mine, E.; Nagao, D.; Konno, M.; Liz-Marzán, L. M. *J. Colloid Interface Sci.* **2005**, *283*, 392.
(46) Selvan, S. T.; Tan, T. T.; Ying, J. Y. *Adv. Mater.* **2005**, *17*, 1620.
(47) (a) Bagwe, R. P.; Zhao, X.; Tan, W. *J. Disp. Sci. Technol.* **2003**, *24*, 453. (b) Badley, R. D.; Ford, W. T.; McEnroe, F. J.; Assink, R. A. *Langmuir* **1990**, *6*, 792.
(48) Collinson, M. M. *Trends Anal. Chem.* **2002**, *21*, 30.

(49) Rossi, L. M.; Silva, P. R.; Vono, L. L. R.; Fernandes, A. U.; Tada, D. B.; Baptista, M. S. *Langmuir* **2008**, *24*, 12534.
(50) Zhao, X.; Tapec-Dytioco, R.; Tan, W. *J. Am. Chem. Soc.* **2003**, *125*, 11474.
(51) Brondani, D.; Vieira, I. C.; Piovezan, C.; da Silva, J. M. R.; Neves, A.; Dupont, J.; Scheeren, C. W. *Analyst* **2010**, *135*, 1015.
(52) Collect Enraf-Nonius, Nonius BV, Delft, The Netherlands, 1997−2000.
(53) Otwinowski, Z.; Minor, W. *Macromol. Crystallogr.* **1997**, *276* (Pt.A), 307.
(54) Altomare, A.; Burla, M. C.; Camalli, M.; Cascarano, G. L.; Guagliardi, C.; Moliterni, A.; Polidori, G.; Spagna, R. *J. Appl. Crystallogr.* **1999**, *32*, 115.
(55) Sheldrick, G. M. *Acta Crystallogr., Sect. A: Found. Crystallogr.* **2008**, *A64*, 112.
(56) Herrador, M. A.; Gonzalez, A. G. *Talanta* **2002**, *56*, 769.
(57) Martell, A. E.; Motekaitis, R. J. *Determination and Use of Stability Constants*, 2nd ed.; VHC Publishers, Inc.: Weinheim, Germany, 1992.
(58) Karsten, P.; Neves, A.; Bortoluzzi, A. J.; Lanznaster, M.; Drago, V. *Inorg. Chem.* **2002**, *41*, 4624.
(59) Bunton, C. A.; Farber, S. J. *J. Org. Chem.* **1969**, *34*, 767.
(60) Konrad, M.; Meyer, F.; Jacobi, A.; Kircher, P.; Rutsch, P.; Zsolnai, L. *Inorg. Chem.* **1999**, *38*, 4559.
(61) Yajima, T.; Okajima, M.; Odani, A.; Yamauchi, O. *Inorg. Chim. Acta* **2002**, *339*, 445.
(62) Nakamoto, K. *Infrared and Raman Spectra of Inorganic and Coordination Compounds*, 5th ed.; John Wiley and Sons, Ltd.: New York, 1997.
(63) Geary, W. J. *Coord. Chem. Rev.* **1971**, *7*, 81.
(64) Lanznaster, M.; Neves, A.; Bortoluzzi, A. J.; Szpoganicz, B.; Schwingel, E. *Inorg. Chem.* **2002**, *41*, 5641.
(65) Lambert, E.; Chabut, B.; Chardon-Noblat, S.; Deronzier, A.; Chottard, G.; Bousseksou, A.; Tuchagues, J. P.; Laugier, J.; Bardet, M.; Latour, J. M. *J. Am. Chem. Soc.* **1997**, *119*, 9424.
(66) Rotthaus, O.; Thomas, F.; Jarjayes, O.; Philouze, C.; Saint-Aman, E.; Pierre, J.-L. *Eur. J. Inorg. Chem.* **2006**, *12*, 6953.
(67) Chaudhuri, P.; Wagner, R.; Khanra, S.; Weyhermuller, T. *Dalton Trans.* **2006**, 4962.
(68) Ylma, G. *Polyhedron* **1998**, *17*, 3351.
(69) Osório, R. E. H. M. B.; Peralta, R. A.; Bortoluzzi, A. J.; de Almeida, V. R.; Szpoganicz, B.; Fischer, F. L.; Terenzi, H.; Mangrich, A. S.; Mantovani, K. M.; Ferreira, D. E. C.; Rocha, W. R.; Haase, W.; Tomkowicz, Z.; Dos Anjos, A.; Neves, A. *Inorg. Chem.* **2012**, *51*, 1569.
(70) Greatti, A.; de Brito, M. A.; Bortoluzzi, A. J.; Ceccato, A. S. *J. Mol. Struct.* **2004**, *688*, 185.
(71) Loloee, R.; Chavez, F. A.; Pawlak, P. L.; Malkhasian, A. Y. S.; Sjlivic, B.; Tiza, M. J.; Kucera, B. E. *Inorg. Chem. Commun.* **2008**, *11*, 1023.
(72) Neves, A.; Lanznaster, M.; Bortoluzzi, A. J.; Peralta, R. A.; Casellato, A.; Castellano, E. E.; Herrald, P.; Riley, M. J.; Schenk, G. *J. Am. Chem. Soc.* **2007**, *129*, 7486.
(73) Burstyn, J. N.; Deal, K. A.; Hengge, A. C. *J. Am. Chem. Soc.* **1996**, *118*, 1713.
(74) Gold, V. *Advances in Physical Organic Chemistry*; Academic Press: New York, 1967.